Deterministic generation of hybrid high-N NOON states with Rydberg atoms trapped in microwave cavities

Naeimeh Mohseni,[1,2,*] Shahpoor Saeidian,[1,†] Jonathan P. Dowling,[3,4,5,6,‡] and Carlos Navarrete-Benlloch[2,7,§]

[1]*Department of Physics, Institute for Advanced Studies in Basic Sciences (IASBS), Iran*
[2]*Max-Planck-Institut für die Physik des Lichts, Staudtstrasse 2, 91058 Erlangen, Germany*
[3]*Hearne Institute for Theoretical Physics and Department of Physics and Astronomy, Louisiana State University, Baton Rouge, Louisiana 70803, USA*
[4]*CAS-Alibaba Quantum Computing Laboratory, USTC, Shanghai 201315, China*
[5]*NYU-ECNU Institute of Physics at NYU Shanghai, Shanghai 200062, China*
[6]*National Institute of Information and Communications Technology, Tokyo 184-8795, Japan*
[7]*Wilczek Quantum Center, School of Physics and Astronomy, Shanghai Jiao Tong University, Shanghai 200240, China*

(Received 26 September 2018; revised manuscript received 30 September 2019; published 8 January 2020)

Trapped atoms are among the most promising platforms for quantum technologies. They play a remarkable role in quantum simulation as well as high-precision quantum metrology, which exploits the quantum coherence of a single electronic or motional degree of freedom of an atom or an ensemble. However, future high-precision quantum metrology will require the use of entangled states of several degrees of freedom. Here we propose a protocol capable of generating high-N NOON states where the entanglement is shared between the motion of a trapped atom and an electromagnetic cavity mode, a so-called "hybrid" configuration. We explore the feasibility of the proposal in a platform consisting of an optically trapped neutral atom excited to its circular-Rydberg-state manifold, coupled to the modes of a high-Q microwave cavity. This compact hybrid architecture has the advantage that it can couple to signals of very different nature, which modify either the atom's motion or the cavity modes. Moreover, the exact same setup can be used right after the state-preparation phase to implement the interferometer required for quantum metrology.

DOI: 10.1103/PhysRevA.101.013804

I. INTRODUCTION

Trapped neutral atoms are at the forefront of quantum technological applications. They are currently the main platform for quantum simulation [1–9] and find applications in many other quantum information processing tasks [10–12]. Furthermore, trapped atoms play a notable role in metrological applications [13,14], thanks to their robust quantum coherence, high controllability, and strong coupling with external fields. For example, an optical lattice loaded with ^{87}Sr forms the basis for the most precise clock built to date [15,16].

However, moving forward in the field of quantum metrology will require exploiting more than just the quantum coherence of a single degree of freedom. Indeed, it is by now well established that distributing entanglement among several degrees of freedom can bring sensitivities all the way down to the ultimate Heisenberg limit [13,17,18]. In this regard, NOON states of two oscillators and Greenberger-Horne-Zeilinger (GHZ) states of N two-level systems are among the most promising entangled states. GHZ states have enjoyed a more successful experimental life, with states up to $N = 20$, 14, and 10 generated with atomic arrays [19], ion chains [20], and linear optics [21], respectively. However, their use in quantum metrology requires the coherent manipulation of the large number of two-level systems, as well as their common coupling to the signal one wants to measure. In contrast, NOON states require the manipulation of just two harmonic modes (and only one of them has to couple to the signal), and are therefore more desirable in general. Unfortunately, high-N NOON states have traditionally been more elusive. In the photonic case, the largest NOON state to date has $N = 5$ [22]. In the case of motional states of trapped atoms, a big step forward has been recently achieved with the generation of an $N = 9$ state of two motional modes of a single ion [23].

If trapped atoms are to also come ahead in this new "entangled metrological era," we will need to design further practical protocols for the generation of high-N NOON states, either between atomic degrees of freedom or between an atom and some other system, in what are dubbed "hybrid" configurations, which might lead to more flexible and versatile meters.

Here we show that a single Rydberg atom tightly trapped by an optical field within a microwave cavity will open the door to the possibility of generating such states. This architecture combines the best of two worlds. On the one hand, in an atomic fly-through configuration [24,25], these systems have been crucial for the field of cavity quantum electrodynamics: high-Q superconducting cavities and microwave transitions

*n.mohseni@iasbs.ac.ir
†saeidian@iasbs.ac.ir
‡jdowling@phys.lsu.edu
§Corresponding author: derekkorg@gmail.com

between Rydberg states have provided access to the deep-strong-coupling regime of light-matter interactions. On the other hand, the tight confinement induced by optical fields [4–8,19,26–41] allows one to apply to neutral atoms all of the well-established toolbox developed for trapped ions [42,43], arguably among the most versatile quantum systems, allowing for the engineering of a large variety of effective interactions between motional, electronic, and photonic degrees of freedom. In this paper, we exploit the combined outstanding properties of these two scenarios to introduce a practical protocol for the generation of hybrid high-N NOON states of an atom and a cavity mode, in a compact architecture that can directly serve as the interferometer required for quantum metrology [17].

Our protocol is inspired by the so-called magic beam splitter [44], which uses N-photon input states, beam splitters, controlled-π phase gates, and on/off detectors as resources. Here we show that a trapped three-level atom interacting with two cavity modes provides all the required ingredients for the realistic implementation of a similar protocol, which we introduce in three steps. First, we propose an implementation of a hybrid beam splitter (HBS) between a cavity mode and a motional mode of the atom, with transmissivity and relative phase fully controllable via the amplitude of an external field and the interaction time. Hence, we call this a "temporal analog" of a HBS. We then show that a second internal transition can be used to generate strong hybrid cross-Kerr effective interactions between the cavity and the atom's motion, which implement the required controlled-phase gate. These operations are then combined with other standard ones and with the possibility of creating high-N Fock states in the atom's motion [45–48] or in the microwave mode [49–52] to show that three internal levels, together with a simple design of external drives and cavity interactions, suffice to implement a temporal analog of a magic beam splitter.

At the end, we briefly comment on specific metrological applications, emphasizing that our hybrid NOON states provide a switchable photonic or mechanical architecture that is sensitive to signals of very different nature. Moreover, the hybrid Mach-Zehnder interferometer required for quantum enhanced metrology [17] can be directly implemented with the same tools introduced for the NOON state generation.

II. TEMPORAL ANALOG OF A HYBRID BEAM SPLITTER

Let us consider an atom of mass m cooled to the ground state of a harmonic optical trap with trapping frequency ν (we consider an isolated motional mode) [8,28,30,31]. We assume that the atom has been excited to a long-lived circular Rydberg state [8,24], and consider the transition between two of such internal states $|g\rangle$ and $|e_1\rangle$ with frequency difference ω_0. The atom is inside a microwave cavity and hence interacts with its standing-wave modes, of which we consider here a specific one with frequency ω_1. The cavity field is pumped by a coherent microwave source at frequency $\omega_{\rm p}$ (see the energy-level scheme in Fig. 1). In a picture rotating at this frequency, the Hamiltonian reads [53]

$$\hat{H} = \hbar\nu\hat{a}^\dagger\hat{a} + \hbar\Delta_0\hat{\sigma}_1^\dagger\hat{\sigma}_1 + \hbar\Delta_1\hat{b}_1^\dagger\hat{b}_1 - \hbar(\mathcal{E}^*\hat{b}_1 + \mathcal{E}\hat{b}_1^\dagger) + \hbar g(\hat{x})(\hat{\sigma}_1^\dagger\hat{b}_1 + \hat{\sigma}_1\hat{b}_1^\dagger), \quad (1)$$

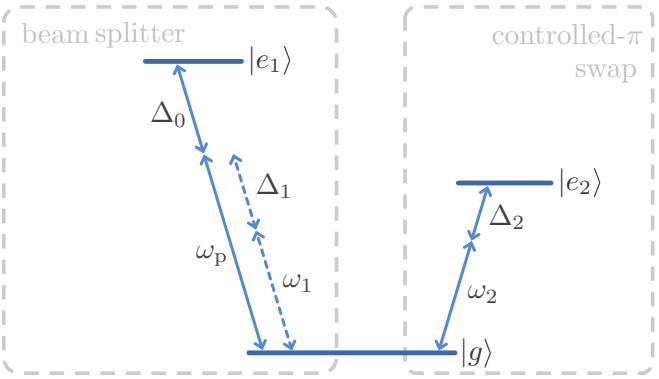

FIG. 1. Energy-level scheme of a three-level atom interacting with the cavity modes. The first transition is used to implement a hybrid beam splitter when $|\Delta_0| \gg \Delta_1 = \nu$. The second transition is used to implement a hybrid controlled-π operation when $|\Delta_2|$ is large or a swap operation (through a resonant Jaynes-Cummings interaction) when it is zero. Here we assume that the detunings $\Delta_{1,2}$ are tunable at real time, as explained in the text.

where $\hat{b}_1$ and $\hat{a}$ annihilate, respectively, cavity photons and motional quanta (phonons), $\hat{\sigma}_1 = |g\rangle\langle e_1|$ is the lowering operator of the internal transition, $\mathcal{E}$ is the strength of the pump, which is detuned by $\Delta_j = \omega_j - \omega_{\rm p}$ from the corresponding frequency, $g(\hat{x}) = \Omega\sin(\eta\hat{x} + \Phi)$, where Ω is the atom-cavity coupling strength (vacuum Rabi frequency), $\hat{x} = \hat{a} + \hat{a}^\dagger$, and $\Phi = \omega_1 x_0/c$, where x_0 is the position of the atom relative to a node of the standing wave. η is the Lamb-Dicke parameter, given by the ratio between the zero-point spatial fluctuations of the atom in the trap and the mode wavelength. Since we work with microwave modes, the bare η is exceedingly small [54–64], but it can be greatly enhanced via state-dependent optical traps [65–68], as we will discuss in the final section.

We consider the large-atomic-detuning limit ($|\Delta_0| \gg \Omega, |\Delta_1|, \nu$), where the internal levels can be adiabatically eliminated [69]. In Appendix A, we show that this leads to an effective Hamiltonian,

$$\hat{H}_{\rm OM} = \hbar\nu\hat{a}^\dagger\hat{a} + \hbar[\Delta_1 - g_0(\hat{a} + \hat{a}^\dagger)]\hat{b}_1^\dagger\hat{b}_1 - \hbar(\mathcal{E}^*\hat{b}_1 + \mathcal{E}\hat{b}_1^\dagger), \quad (2)$$

where we have defined $g_0 = \eta\Omega^2/2\Delta_0$ and have assumed that the atom is located in between a node and an antinode ($\Phi = \pi/4$), which maximizes this effective coupling. This Hamiltonian is equivalent to that found in cavity quantum optomechanics [70].

Including optical and motional damping at rates γ and Γ, respectively, the master equation governing the evolution of the system can be written as

$$\frac{d\hat{\rho}}{dt} = \left[\frac{\hat{H}_{\rm OM}}{i\hbar}, \hat{\rho}\right] + \gamma\mathcal{D}_{b_1}[\hat{\rho}] + \Gamma\mathcal{D}_a[\hat{\rho}], \quad (3)$$

with dissipator $\mathcal{D}_J[\hat{\rho}] = 2\hat{J}\hat{\rho}\hat{J}^\dagger - \hat{\rho}\hat{J}^\dagger\hat{J} - \hat{J}^\dagger\hat{J}\hat{\rho}$. As we show in Appendix B, the classical limit predicts a coherent state with amplitudes α and β for the motional and optical modes, satisfying

$$\dot{\alpha} = -(\Gamma + i\nu)\alpha + ig_0|\beta|^2, \quad (4a)$$

$$\dot{\beta} = -[\gamma + i\Delta_1 - ig_0(\alpha + \alpha^*)]\beta + i\mathcal{E}. \quad (4b)$$

We will work under conditions leading to a steady state $\bar{\alpha} = g_0|\bar{\beta}|^2/(\nu - i\Gamma)$ and $\bar{\beta} = \mathcal{E}/[\Delta_1 - g_0(\bar{\alpha} + \bar{\alpha}^*) - i\gamma]$. Next, we consider small quantum fluctuations around it by moving to a picture displaced to the classical solution and considering only terms in the master equation bilinear in annihilation and creation operators; see Appendix B. In this picture, the transformed state evolves according to Eq. (3), but replacing the effective Hamiltonian by

$$\hat{H}_{\rm LIN} = \hbar\nu\hat{a}^\dagger\hat{a} + \hbar\Delta_1\hat{b}_1^\dagger\hat{b}_1 - \hbar g_0(\hat{a} + \hat{a}^\dagger)(\bar{\beta}^*\hat{b}_1 + \bar{\beta}\hat{b}_1^\dagger). \quad (5)$$

As we show in Appendix B, this "linearization" is valid provided that $|\beta|$ or ν/g_0 are much larger than $\sqrt{N}$, where N characterizes the photon number $\langle\hat{b}_1^\dagger\hat{b}_1\rangle$ in the displaced picture (which we anticipate matches the size of the NOON state).

Finally, choosing a detuning $\Delta_1 = \nu$ and working in the $\nu \gg g_0|\bar{\beta}|$ regime, this Hamiltonian takes the form

$$\hat{H}_{\rm BS} = \hbar\nu(\hat{a}^\dagger\hat{a} + \hat{b}_1^\dagger\hat{b}_1) - \hbar g_0(\bar{\beta}\hat{a}\hat{b}_1^\dagger + \bar{\beta}^*\hat{a}^\dagger\hat{b}_1), \quad (6)$$

within the rotating-wave approximation. The corresponding time evolution operator corresponds to a HBS operation whose mixing angle $\theta = g_0|\bar{\beta}|t$ and phase $\arg\{\bar{\beta}\}$ (assumed $\pi/2$ in order to simplify upcoming derivations without loss of generality) can be controlled via the interaction time and the pump amplitude $\mathcal{E}$. Note, however, that the performance is limited by the coherence time of the system, which we can estimate as γ^{-1}, typically much shorter than Γ^{-1} [8,24]. Later we show that Rydberg atoms trapped in microwave cavities allow for coherence times that are compatible with the mixing angle $\theta = \pi/4$ required in our proposal.

III. TEMPORAL ANALOG OF A HYBRID CONTROLLED-PHASE GATE

We now consider the interaction between the atom and a second cavity mode with frequency ω_2, closer to resonance with a transition to a different excited state $|e_2\rangle$, but still detuned by Δ_2 (see Fig. 1). The Hamiltonian takes the form (1), which, assuming the atom to be located at the antinode of the cavity mode ($\Phi = \pi/2$), leads to

$$\hat{H} = \hbar\nu\hat{a}^\dagger\hat{a} + \hbar\Delta_2\hat{b}_2^\dagger\hat{b}_2 + \hbar\Omega\cos(\eta\hat{x})(\hat{\sigma}_2^\dagger\hat{b}_2 + \hat{\sigma}_2\hat{b}_2^\dagger), \quad (7)$$

where in this case we are in a picture rotating at the frequency of the internal transition, and $\hat{b}_2$ and $\hat{\sigma}_2$ refer to the corresponding cavity mode and internal transition. In Appendix A, we show that working in the $\nu \gg |\Delta_2| \gg \Omega$ regime, the adiabatic elimination of the internal levels leads to the effective hybrid cross-Kerr interaction [71],

$$\hat{H}_{\rm cK} = \hbar\nu\hat{a}^\dagger\hat{a} + \hbar\Delta_2\hat{b}_2^\dagger\hat{b}_2 - \hbar g_{\rm cK}\hat{a}^\dagger\hat{a}\hat{b}_2^\dagger\hat{b}_2, \quad (8)$$

where $g_{\rm cK} = 2\eta^2\Omega^2/\Delta_2$. In this case, the time-evolution operator is equivalent to a controlled-phase operation, where one mode feels a phase shift that depends on the number of photons of the other. The cross-phase shift $g_{\rm cK}t$ can be controlled in this case through the interaction time. A π shift requires $g_{\rm cK} > \gamma$, whose feasibility is proven later.

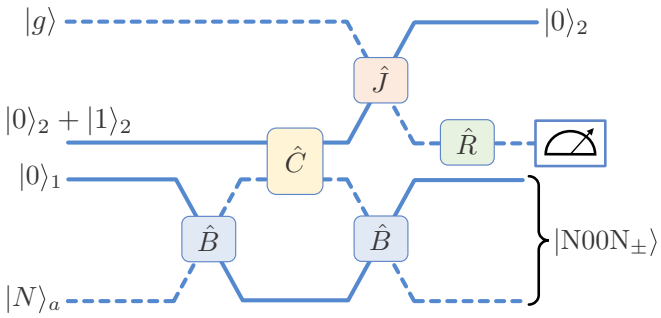

FIG. 2. Schematic representation of the protocol for the generation of NOON states. a refers to the atom's motion, subindices $\{1, 2\}$ to the cavity modes, $\hat{B}$ to a 50/50 beam splitter, $\hat{C}$ to a controlled-π, $\hat{J}$ to a swap, and $\hat{R}$ to a $\pi/4$ pulse. A final measurement of the internal state of the atom ($|g\rangle$ or $|e_2\rangle$) creates the desired NOON state.

IV. HIGH-N NOON STATE GENERATION PROTOCOL

Our proposal is shown in Fig. 2, which is closely inspired by the so-called magic beam splitter [44]. In order to understand its principle of operation, let us first consider a situation without the controlled-π operation $\hat{C}$ (yellow box in the figure), and follow the paths 1 and a, which run along a Mach-Zehnder interferometer. With no more elements in the paths, the combination of the beam splitters acts as a swap gate between the modes. Hence, starting with a Fock state with N phonons for definiteness (but the protocol works as well starting with N photons instead), the state $|0\rangle_1|N\rangle_a$ turns into $|N\rangle_1|0\rangle_a$ (subindex a refers to the motional Fock states, while subindices $\{1, 2\}$ refer to the cavity modes). The situation is radically different when a π phase shift is performed on path a in between the beam splitters, which completely cancels the effect of the latter. In such case, the input state remains unchanged. Hence, if one was able to engineer a balanced superposition of 0 and π phase shifts, the output state would turn into a superposition of $|N\rangle_1|0\rangle_a$ and $|0\rangle_1|N\rangle_a$, that is, a NOON state. This is exactly what is accomplished by the controlled-π operation with mode 2 (assumed in a superposition of 0 and 1 photons), together with the subsequent operations involving the second internal atomic transition. A final measurement revealing the state of the atom decides the relative phase between the $|N\rangle_1|0\rangle_a$ and $|0\rangle_1|N\rangle_a$ states forming the NOON state. In the remainder of this section, we explain all these steps in detail. In the next section, we will then comment on the experimental requirements and their feasibility.

Recall that a balanced beam splitter acts as the unitary $\hat{B} = \exp[\pi(\hat{a}^\dagger\hat{b}_1 - \hat{a}\hat{b}_1^\dagger)/4]$, which transforms the operators as $\hat{B}\hat{a}\hat{B}^\dagger = (\hat{b}_1 + \hat{a})/\sqrt{2}$ and $\hat{B}\hat{b}_1\hat{B}^\dagger = (\hat{b}_1 - \hat{a})/\sqrt{2}$. Hence, applied to the initial state $|0\rangle_1|N\rangle_a(|0\rangle_2 + |1\rangle_2)|g\rangle$ (we omit normalizations in the following to ease the notation), we obtain

$$(\hat{b}_1^\dagger + \hat{a}^\dagger)^N|0\rangle_1|0\rangle_a(|0\rangle_2 + |1\rangle_2)|g\rangle. \quad (9)$$

Next we apply the controlled-π with unitary $\hat{C} = \exp(i\pi\hat{b}_2^\dagger\hat{b}_2\hat{a}^\dagger\hat{a})$, which turns the state into

$$(\hat{b}_1^\dagger + \hat{a}^\dagger)^N|0\rangle_1|0\rangle_a|0\rangle_2|g\rangle + (\hat{b}_1^\dagger - \hat{a}^\dagger)^N|0\rangle_1|0\rangle_a|1\rangle_2|g\rangle, \quad (10)$$

where we have used $e^{i\pi\hat{a}^\dagger\hat{a}}\hat{a}e^{-i\pi\hat{a}^\dagger\hat{a}} = -\hat{a}$. A further beam splitter $\hat{B}$ then turns the state into

$$|0\rangle_1|N\rangle_a|0\rangle_2|g\rangle + (-1)^N|N\rangle_1|0\rangle_a|1\rangle_2|g\rangle. \tag{11}$$

Finally, we apply two operations that involve the internal levels. First, we apply an excitation swap between the second cavity mode and the corresponding transition, with unitary $\hat{J} = \exp[-i\pi(\hat{b}_2^\dagger\hat{\sigma}_2 + \hat{b}_2\hat{\sigma}_2^\dagger)/2]$, which performs the transformations $\hat{J}|0\rangle_2|g\rangle = |0\rangle_2|g\rangle$ and $\hat{J}|1\rangle_2|g\rangle = -i|0\rangle_2|e\rangle$. Then, we apply a $\pi/4$ pulse on the internal transition, with corresponding unitary $\hat{R} = \exp[\pi(\hat{\sigma}_2^\dagger - \hat{\sigma}_2)/4]$, and transformations $\hat{R}|g\rangle = |g\rangle + |e\rangle$ and $\hat{R}|e\rangle = |e\rangle - |g\rangle$. These turn the state into

$$|\mathrm{NOON}_+\rangle|0\rangle_2|g\rangle + |\mathrm{NOON}_-\rangle|0\rangle_2|e\rangle, \tag{12}$$

where we have defined the hybrid NOON states $|\mathrm{NOON}_\pm\rangle = |0\rangle_1|N\rangle_a \pm i(-1)^N|N\rangle_1|0\rangle_a$. It is then clear that a final measurement of the atomic state will project the atom and the first cavity mode into a $|\mathrm{NOON}_\pm\rangle$ state, depending on the outcome.

V. EXPERIMENTAL CONSIDERATIONS AND FEASIBILITY

Let us now comment on the experimental steps and corresponding requirements. We start with some general considerations and then discuss specific parameters.

As we made obvious from the notation, the beam splitters $\hat{B}$ and controlled-π $\hat{C}$ operations are implemented through cavity modes 1 and 2, respectively, following the methods presented in the first sections. The rest of the operations are standard [24]: the swap $\hat{J}$ is performed by letting a resonant Jaynes-Cummings (JC) interaction $\hbar\Omega(\hat{\sigma}_2^\dagger\hat{b}_2 + \hat{\sigma}_2\hat{b}_2^\dagger)$ run over a time $\pi/2\Omega$, while $\hat{R}$ is obtained by driving the second transition with a coherent microwave $\pi/4$ pulse. The crucial point is that since the operations are applied sequentially, we need to be able to switch on and off the corresponding interactions at will. Following [72], here we suggest to do so by modifying the corresponding atom-cavity detunings Δ_0 and Δ_2 in real time. Specifically, the frequency of the atomic transition can be tuned *in situ* and fast through either the dc Stark, Zeeman, or ponderomotive shifts generated, respectively, by external electrostatic [24,72], magnetostatic [42,73], or optical [36] fields.

Another crucial piece is the preparation of the initial states. Specifically, in order to generate *high-N* NOON states, we need to initialize either the cavity mode 1 or the atom's motion in a Fock state with large N. While this has been demonstrated for both alternatives, the relatively strong coherent background $\bar{\beta}$ required for the beam-splitter operation makes it challenging to adapt the established protocols for microwave cavities, where photonic Fock states up to $N = 7$ have been stabilized via quantum feedback techniques [49–51]. Fortunately, the (comparatively small) steady-state amplitude $\bar{\alpha}$ of the trapped atom poses no problem since it just defines a new stationary equilibrium position, but no oscillation. Moreover, Fock states of trapped ions up to $N = 16$ were demonstrated in trapped ions more than 20 years ago [45], proving that this is a very mature field (see [46–48] for more modern and elaborated experiments). The corresponding protocols exploit the fact that the interaction between motion and internal states can be alternated between JC and anti-JC at will, what makes them directly applicable to our proposal, where this is equally possible. As for the preparation of cavity mode 2 in a superposition of 0 and 1 photons, it can be easily performed following techniques that have become standard in the field of cavity quantum electrodynamics [24]. For example, one can apply the inverse of the $\hat{R}\hat{J}$ sequence that we perform at the end of our protocol: starting from the atom in the ground state, a $\pi/4$ pulse is applied, followed by a swap of the internal excitation to the cavity field. Note that this state-preparation stage must come only once the system relaxes to the steady state after application of the microwave drive, and under large detuning conditions such that no other process acts during this time.

Finally, the measurement of the internal atomic state can be performed following standard techniques in the field of trapped atoms and ions [42]. Hence, together with the previous discussion, this shows that all the pieces required for the implementation of the high-N NOON protocol presented above are, in principle, available.

Let us now move on to the feasibility for concrete experimental parameters. The most demanding operation is the controlled-π, which requires the conditions $\nu \gg |\Delta_2| \gg \Omega$ together with $g_{\mathrm{cK}} = 2\eta^2\Omega^2/|\Delta_2| > \gamma$ in order to ensure that the coherence time is large enough to implement a π shift. Taking cavity frequencies and quality factors around $2\pi \times$ 50 GHz [24,72] and 5×10^9 [52,72], respectively, we obtain $\gamma = 2\pi \times 10$ Hz. On the other hand, typical vacuum Rabi couplings for transitions between circular Rydberg states are around $\Omega = 2\pi \times 50$ KHz [24,72]. We then assume $|\Delta_2| = 10\Omega$, and a trapping frequency $\nu = 10|\Delta_2| = 2\pi \times 5$ MHz (values just two orders of magnitude below this have been demonstrated already [8,41] and no fundamental limitation exists to bring them even higher, as shown in [38]). As for the Lamb-Dicke parameter, we assume the value $\eta = 0.1$, which is currently available with the aid of state-dependent trapping potentials [65–68]. Putting all these estimates together, we obtain $g_{\mathrm{cK}} = 10\gamma$, as required.

The rest of the operations are less demanding. The effective beam-splitter Hamiltonian requires $|\Delta_0| \gg \nu \gg g_0\max\{\sqrt{N}, |\bar{\beta}|\}$, together with $g_0|\bar{\beta}| \gg \gamma$. Taking $|\Delta_0| = 10\nu$, we obtain $g_0 = 2\pi \times 5$ Hz. The number of intracavity photons $|\bar{\beta}|^2$ generated by the coherent microwave pump is then bounded by $(\nu/g_0)^2 = 10^{12} \gg |\bar{\beta}|^2 \gg (\gamma/g_0)^2 = 4$. Choosing it between, e.g., 500 and 10 000 (photon numbers easily generated with coherent pumps), we remain safely within the desired regime. As for the swap operation, we simply need $\Omega \gg \max\{\gamma, \Gamma_e\}$, where Γ_e refers to the spontaneous-emission rate associated to the internal transition. For circular Rydberg states, the latter is typically even smaller than γ [8,24], and hence we are deep into the required regime.

We have also analyzed the resilience of our proposal to parameter fluctuations. We have considered fluctuations in the beam splitter and controlled-π parameters, finding analytic expressions for the fidelity; see Appendix C for details. As a figure of merit, we find fidelities above 90% up to $N = 40$ for a 1% standard deviation in the parameters.

VI. DISCUSSION AND CONCLUSIONS

Our compact architecture offers interesting opportunities from a metrological standpoint. Its hybrid character makes it a versatile sensor, i.e., sensitive to signals that couple either to the cavity or to the atom's motion. Specifically, right after generating the NOON state, the same setup can be used to implement the temporal analog of the Mach-Zehnder interferometer required for metrology [17]: a hybrid beam-splitter interaction is implemented for the required time following our proposal, after which the atom or the cavity is coupled to the signal we wish to measure (which introduces a measurable phase difference between them), and then decoupled again from the signal before the optimal retrieval measurement scheme is applied [17,18].

In conclusion, we have shown that an architecture based on trapped atoms excited to circular Rydberg states and coupled to the modes of a microwave cavity will be ideal for the compact implementation of a versatile quantum metrological system, where the state preparation and sensing stages occur within the same device.

ACKNOWLEDGMENTS

We thank Marjan Fani for useful discussions. N.M. was partially supported by the Ministry of Science Research and Technology of Iran and IASBS (Grant No. G 2018 IASBS 12648). J.P.D. would like to acknowledge support from the U.S. Air Force Office of Scientific Research, the U.S. Army Research Office, the Defense Advanced Projects Activity, the National Science Foundation, and the Northrop Grumman Corporation. C.N.B. acknowledges additional support from a Shanghai talent program.

APPENDIX A: ADIABATIC ELIMINATION OF THE INTERNAL LEVELS

In this Appendix, we provide a detailed elimination of the internal levels. We will proceed in the Schrödinger picture, using the method based on projection operators. Hence, we first introduce the general method, which we then particularize to the two relevant internal transitions.

1. General procedure: Projection operator method

Let us introduce, in general, the method based on projection operators. Consider a closed system evolving according to a Hamiltonian $\hat{H}$, so that its state $|\psi(t)\rangle$ satisfies the Schrödinger equation $i\hbar\partial_t|\psi(t)\rangle = \hat{H}|\psi(t)\rangle$. The idea of the method relies on the fact that we can divide the Hilbert space into a relevant sector (whose effective dynamics we want to describe) and an irrelevant one (whose dynamics is trivial, typically because it stays unpopulated). We then define the projector operator $\hat{P} = \hat{P}^2$, which projects onto the relevant subspace, and its complement $\hat{Q} = 1 - \hat{P}$. Applying the latter onto the Schrödinger equation, we get

$$\begin{aligned} i\hbar\partial_t\hat{Q}|\psi(t)\rangle &= \hat{Q}\hat{H}(\underbrace{\hat{P}+\hat{Q}}_{1})|\psi(t)\rangle \\ &= \hat{Q}\hat{H}\hat{Q}|\psi(t)\rangle + \hat{Q}\hat{H}\hat{P}|\psi(t)\rangle, \end{aligned} \tag{A1a}$$

$$\Downarrow$$

$$\begin{aligned} \hat{Q}|\psi(t)\rangle &= \frac{1}{i\hbar}e^{\hat{Q}\hat{H}t/i\hbar}\hat{Q}|\psi(0)\rangle \\ &\quad + \int_0^t \frac{dt'}{i\hbar}e^{\hat{Q}\hat{H}(t-t')/i\hbar}\hat{Q}\hat{H}\hat{P}|\psi(t')\rangle. \end{aligned} \tag{A1b}$$

Naturally, we assume that the system is in the relevant subspace initially, so that $\hat{Q}|\psi(0)\rangle = 0$. Hence, projecting the Schrödinger equation in the relevant subspace, we then obtain

$$\begin{aligned} i\hbar\partial_t\hat{P}|\psi(t)\rangle &= \hat{P}\hat{H}\hat{P}|\psi(t)\rangle + \hat{P}\hat{H}\hat{Q}|\psi(t)\rangle \\ &= \hat{P}\hat{H}\hat{P}|\psi(t)\rangle \\ &\quad + \int_0^t \frac{d\tau}{i\hbar}\hat{P}\hat{H}e^{\hat{Q}\hat{H}\tau/i\hbar}\hat{Q}\hat{H}\hat{P}|\psi(t-\tau)\rangle, \end{aligned} \tag{A2}$$

where we have made the integration variable change $t' = t - \tau$.

With full generality, we can decompose the Hamiltonian as $\hat{H} = \hat{H}_0 + \hat{H}_1$, where $\hat{H}_0$ contains all the terms that do not connect the relevant and irrelevant subspaces ($\hat{P}\hat{H}_0\hat{Q} = 0 = \hat{Q}\hat{H}_0\hat{P}$), while $\hat{H}_1$ gathers the rest of the terms. Note that we can even assume without loss of generality that $\hat{P}\hat{H}_1\hat{P} = 0$, that is, the "interaction" Hamiltonian $\hat{H}_1$ does not connect states within the relevant subspace. It is always possible to ensure such a property, for if that is not the case, we just need to redefine $\hat{H}_0$ and $\hat{H}_1$ as $\hat{H}_0 + \hat{P}\hat{H}_1\hat{P}$ and $\hat{H}_1 - \hat{P}\hat{H}_1\hat{P}$, respectively. Effective theories are meaningful whenever one can treat $\hat{H}_1$ as a perturbation with respect to $\hat{H}_0$. Hence, in the following, we consider only terms up to second order in $\hat{H}_1$ in (A2). In order to do this, we use $|\psi(t-\tau)\rangle = e^{-\hat{H}\tau/i\hbar}|\psi(t)\rangle$ and the property $\hat{P}\hat{H}_0\hat{Q} = 0 = \hat{Q}\hat{H}_0\hat{P}$, which allows us to write (A2) as

$$\begin{aligned} &i\hbar\partial_t\hat{P}|\psi(t)\rangle \\ &= \hat{P}\hat{H}\hat{P}|\psi(t)\rangle + \int_0^t \frac{d\tau}{i\hbar}\hat{P}\hat{H}_1e^{\hat{Q}\hat{H}\tau/i\hbar}\hat{Q}\hat{H}_1\hat{P}e^{-\hat{H}\tau/i\hbar}|\psi(t)\rangle \\ &= \left[\hat{P}\hat{H}\hat{P} + \int_0^t \frac{d\tau}{i\hbar}\hat{P}\hat{H}_1e^{\hat{H}_0\tau/i\hbar}\hat{H}_1e^{-\hat{H}_0\tau/i\hbar}\hat{P}\right]\hat{P}|\psi(t)\rangle, \end{aligned} \tag{A3}$$

where in the last step we have made many simplifications. First, we have neglected the $\hat{H}_1$ terms coming from the exponentials since the expression is already quadratic in $\hat{H}_1$ without counting these terms. We have also made use of $[\hat{P},\hat{H}_0] = 0 = [\hat{Q},\hat{H}_0]$, which follows directly from $0 = \hat{P}\hat{H}_0\hat{Q} - \hat{Q}\hat{H}_0\hat{P} = \hat{P}\hat{H}_0(\hat{1}-\hat{P}) - (\hat{1}-\hat{P})\hat{H}_0\hat{P} = [\hat{P},\hat{H}_0]$, and can be used to prove the property

$$\begin{aligned} e^{\hat{Q}\hat{H}_0\tau/i\hbar} &= \sum_{k=0}^{\infty}\frac{1}{k!}\left(\frac{\tau}{i\hbar}\right)^k\underbrace{\hat{Q}\hat{H}_0\hat{Q}\hat{H}_0\ldots\hat{Q}\hat{H}_0}_{k\text{ times}} \\ &= \sum_{k=0}^{\infty}\frac{1}{k!}\left(\frac{\tau}{i\hbar}\right)^k\underbrace{\hat{Q}^k}_{\hat{Q}}\hat{H}_0^k = \hat{Q}e^{\hat{H}_0\tau/i\hbar}. \end{aligned} \tag{A4}$$

Finally, we have used $\hat{P}\hat{H}_1\hat{Q} = \hat{P}\hat{H}_1(1-\hat{P}) = \hat{P}\hat{H}_1$ and, similarly, $\hat{Q}\hat{H}_1\hat{P} = \hat{H}_1\hat{P}$. The term inside the brackets in (A3) can then be interpreted as an effective Hamiltonian in the relevant subspace, which we can write in the compact form

$$\hat{H}_{\text{eff}}(t) = \hat{P}\hat{H}_0\hat{P} + \int_0^t \frac{d\tau}{i\hbar}\hat{P}\hat{H}_1\tilde{H}_1(\tau)\hat{P}, \tag{A5}$$

with

$$\tilde{H}_1(\tau) = e^{\hat{H}_0\tau/i\hbar}\hat{H}_1 e^{-\hat{H}_0\tau/i\hbar}. \tag{A6}$$

This provides the final expression we will work with.

Note that (A5) is not Hermitian, which seems to be at odds with the fact that we interpret it as an effective Hamiltonian. In addition, (A5) is time dependent, even if the original Hamiltonian was time independent. However, in many situations, it indeed occurs that (A5) becomes approximately Hermitian and time independent under the same physical conditions that allow us to split the Hilbert space into relevant and irrelevant subspaces. We will see this in the examples that we treat next.

2. Elimination of $|e_1\rangle$: Effective optomechanical interaction

Let us apply the general framework presented above to the elimination of the first transition of the atom presented in the main text, described by the Hamiltonian (1) that we reproduce here for convenience,

$$\hat{H} = \hbar\nu\hat{a}^\dagger\hat{a} + \hbar\Delta_0\hat{\sigma}_1^\dagger\hat{\sigma}_1 + \hbar\Delta_1\hat{b}_1^\dagger\hat{b}_1 - \hbar(\mathcal{E}^*\hat{b}_1 + \mathcal{E}\hat{b}_1^\dagger) + \hbar g(\hat{x})(\hat{\sigma}_1^\dagger\hat{b}_1 + \hat{\sigma}_1\hat{b}_1^\dagger), \tag{A7}$$

with $g(\hat{x}) = \Omega\sin(\eta\hat{x} + \Phi)$. Assuming that $|\Delta_0| \gg \Omega, |\Delta_1|, \nu, |\mathcal{E}|$, with the atom starting in the ground state $|g\rangle$, we expect the excited state $|e_1\rangle$ to remain unpopulated. Hence, the Hilbert space is naturally divided into a relevant one described by the projector $\hat{P} = |g\rangle\langle g|$ and an irrelevant one with projector $\hat{Q} = 1 - |g\rangle\langle g| = |e_1\rangle\langle e_1|$. Similarly, using the notation of the previous section, the Hamiltonian is naturally split into

$$\hat{H}_0 = \hbar\nu\hat{a}^\dagger\hat{a} + \hbar\Delta_0\hat{\sigma}_1^\dagger\hat{\sigma}_1 + \hbar\Delta_1\hat{c}_1^\dagger\hat{c}_1, \tag{A8a}$$

$$\hat{H}_1 = \hbar g(\hat{x})\left[\hat{\sigma}_1^\dagger\left(\hat{c}_1 + \frac{\mathcal{E}}{\Delta_1}\right) + \hat{\sigma}_1\left(\hat{c}_1^\dagger + \frac{\mathcal{E}^*}{\Delta_1}\right)\right], \tag{A8b}$$

where, for convenience, we have defined the displaced photonic operator $\hat{c}_1 = \hat{b}_1 - \mathcal{E}/\Delta_1$ (hence this Hamiltonian defers from the previous one by a constant shift $|\mathcal{E}|^2/\Delta_1$, irrelevant for the system dynamics). Taking into account that

$$e^{\hat{H}_0\tau/i\hbar}\hat{\sigma}_1 e^{-\hat{H}_0\tau/i\hbar} = e^{i\Delta_0\tau}\hat{\sigma}_1, \tag{A9a}$$

$$e^{\hat{H}_0\tau/i\hbar}\hat{a}e^{-\hat{H}_0\tau/i\hbar} = e^{i\nu\tau}\hat{a}, \tag{A9b}$$

$$e^{\hat{H}_0\tau/i\hbar}\hat{c}_1 e^{-\hat{H}_0\tau/i\hbar} = e^{i\Delta_1\tau}\hat{c}_1, \tag{A9c}$$

we then have

$$\tilde{H}_1(\tau) = e^{\hat{H}_0\tau/i\hbar}\hat{H}_1 e^{-\hat{H}_0\tau/i\hbar} = \hbar g[\tilde{x}(\tau)]e^{-i\Delta_0\tau}\hat{\sigma}_1^\dagger\left(e^{i\Delta_1\tau}\hat{c}_1 + \frac{\mathcal{E}}{\Delta_1}\right) + \text{H.c.}, \tag{A10}$$

with $\tilde{x}(\tau) = e^{i\nu\tau}\hat{a} + e^{-i\nu\tau}\hat{a}^\dagger$. The second-order term of the effective Hamiltonian (A5) then reads

$$\begin{aligned}\int_0^t \frac{d\tau}{i\hbar}\hat{P}\hat{H}_1\tilde{H}_1(\tau)\hat{P} &= -i\hbar g(\hat{x})\left(\hat{c}_1^\dagger + \frac{\mathcal{E}^*}{\Delta_1}\right)\times\int_0^t d\tau g[\tilde{x}(\tau)]e^{-i\Delta_0\tau}\left(e^{i\Delta_1\tau}\hat{c}_1 + \frac{\mathcal{E}}{\Delta_1}\right)|g\rangle\langle g| \\ &\approx -i\hbar g^2(\hat{x})\left(\hat{c}_1^\dagger + \frac{\mathcal{E}^*}{\Delta_1}\right)\left(\hat{c}_1 + \frac{\mathcal{E}}{\Delta_1}\right)\int_0^t d\tau e^{-i\Delta_0\tau}|g\rangle\langle g| \\ &= \hbar\frac{g^2(\hat{x})}{\Delta_0}\hat{b}_1^\dagger\hat{b}_1(e^{-i\Delta_0 t} - 1)|g\rangle\langle g|,\end{aligned} \tag{A11}$$

where we have performed an intermediate approximation neglecting the oscillations at frequencies ν and $|\Delta_1|$ in the time integral, compatible with the fact that the oscillations at $|\Delta_0|$ are much faster (this step is not critical, that is, we can perform the required time integrations including all timescales, but it simplifies the derivation enormously and leads to the same final result in the considered regime). The time dependence of (A11) can be neglected within a rotating-wave approximation as long as $|\Delta_0| \gg \Omega$.

Next we use $\eta \ll 1$ to expand the coupling term as $g^2(\hat{x}) = \Omega^2\sin^2(\eta\hat{x} + \Phi) \approx \Omega^2[\sin^2(\Phi) + \eta\hat{x}\sin(2\Phi)/2]$. Choosing $\Phi = \pi/4$ as mentioned in the main text, we then obtain the final effective Hamiltonian,

$$\hat{H}_{\text{eff}} = \hbar\nu\hat{a}^\dagger\hat{a} + \hbar\left(\Delta_1 - \frac{\Omega^2 + \eta\Omega^2\hat{x}}{2\Delta_0}\right)\hat{b}_1^\dagger\hat{b}_1 - \hbar(\mathcal{E}^*\hat{b}_1 + \mathcal{E}\hat{b}_1^\dagger), \tag{A12}$$

which matches the optomechanical Hamiltonian (2) introduced in the main text. Note that there we made the simplification $|\Delta_1| \gg \Omega^2/2|\Delta_0|$, which is usually very well satisfied.

3. Elimination of $|e_2\rangle$: Effective cross-Kerr interaction

We now apply the method to the second transition of the ion. The corresponding Hamiltonian is described by (7), that is,

$$\hat{H} = \hbar\nu\hat{a}^\dagger\hat{a} + \hbar\Delta_2\hat{b}_2^\dagger\hat{b}_2 + \hbar\Omega\cos(\eta\hat{x})(\hat{\sigma}_2^\dagger\hat{b}_2 + \hat{\sigma}_2\hat{b}_2^\dagger). \tag{A13}$$

In this case, we assume that $\nu \gg |\Delta_2| \gg \Omega$. Hence, for an atom starting in the ground state $|g\rangle$, we again expect the excited state $|e_2\rangle$ to remain unpopulated. Therefore, the projector onto the relevant subspace again reads $\hat{P} = |g\rangle\langle g|$, so that $\hat{Q} = |e_2\rangle\langle e_2|$. We now split the Hamiltonian into

$$\hat{H}_0 = \hbar\nu\hat{a}^\dagger\hat{a} + \hbar\Delta_2\hat{b}_2^\dagger\hat{b}_2, \tag{A14a}$$

$$\hat{H}_1 = \hbar\Omega\cos(\eta\hat{x})(\hat{\sigma}_2^\dagger\hat{b}_2 + \hat{\sigma}_2\hat{b}_2^\dagger). \tag{A14b}$$

Taking into account that

$$e^{\hat{H}_0\tau/i\hbar}\hat{\sigma}_2 e^{-\hat{H}_0\tau/i\hbar} = \hat{\sigma}_2, \tag{A15a}$$

$$e^{\hat{H}_0\tau/i\hbar}\hat{a}e^{-\hat{H}_0\tau/i\hbar} = e^{i\nu\tau}\hat{a}, \tag{A15b}$$

$$e^{\hat{H}_0\tau/i\hbar}\hat{b}_2 e^{-\hat{H}_0\tau/i\hbar} = e^{i\Delta_2\tau}\hat{b}_2, \tag{A15c}$$

we then have

$$\tilde{H}_1(\tau) = e^{\hat{H}_0\tau/i\hbar}\hat{H}_1 e^{-\hat{H}_0\tau/i\hbar} = \hbar\Omega\cos[\eta\tilde{x}(\tau)]e^{i\Delta_2\tau}\hat{\sigma}_2^\dagger\hat{b}_2 + \text{H.c.} \tag{A16}$$

Before proceeding, it is now convenient to use the $\eta \ll 1$ expansion,

$$\cos[\eta\tilde{x}(\tau)] \approx 1 - \eta^2\tilde{x}^2(\tau)/2 \approx 1 - \eta^2\hat{a}^\dagger\hat{a} - \eta^2(e^{2i\nu\tau}\hat{a}^2 + e^{-2i\nu\tau}\hat{a}^{\dagger 2})/2, \tag{A17}$$

so that the second-order term of the effective Hamiltonian (A5) can be written as

$$\begin{aligned}
&\int_0^t \frac{d\tau}{i\hbar}\hat{P}\hat{H}_1\tilde{H}_1(\tau)\hat{P} \\
&= -i\hbar\Omega^2\cos(\eta\hat{x})\hat{b}_2^\dagger\hat{b}_2\int_0^t d\tau\cos[\eta\tilde{x}(\tau)]e^{i\Delta_2\tau}|g\rangle\langle g| \\
&\approx \hbar\Omega^2\cos(\eta\hat{x})\hat{b}_2^\dagger\hat{b}_2\Bigg[(1-\eta^2\hat{a}^\dagger\hat{a})\frac{1-e^{i\hat{\Delta}_2\tau}}{\Delta_2} \\
&\quad -\frac{\eta^2}{2}\frac{1-e^{2i\nu t}}{\Delta_2+2\nu}\hat{a}^2-\frac{\eta^2}{2}\frac{1-e^{2i\nu t}}{\Delta_2-2\nu}\hat{a}^{\dagger 2}\Bigg]|g\rangle\langle g| \\
&\approx \hbar\frac{\Omega^2}{\Delta_2}\hat{b}_2^\dagger\hat{b}_2(1-\eta^2\hat{a}^\dagger\hat{a})^2|g\rangle\langle g|, \qquad \text{(A18)}
\end{aligned}$$

where, in the last approximation, we have made use of the regime $\nu \gg |\Delta_2| \gg \Omega$, which allows us to neglect all terms except the one presented at the end. Combining this with the zeroth-order term, and keeping terms up to second order in η, we obtain the effective Hamiltonian,

$$\hat{H}_{\text{eff}} = \hbar\nu\hat{a}^\dagger\hat{a} + \hbar\Delta_2\left(1+\frac{\Omega^2}{\Delta_2^2}\right)\hat{b}_1^\dagger\hat{b}_1 - \hbar\frac{2\eta^2\Omega^2}{\Delta_2}\hat{b}_2^\dagger\hat{b}_2\hat{a}^\dagger\hat{a}, \qquad \text{(A19)}$$

which matches the cross-Kerr Hamiltonian (8) introduced in the main text, once Ω^2/Δ_2^2 is neglected in the parentheses.

APPENDIX B: LINEARIZATION OF THE OPTOMECHANICAL INTERACTION

In this Appendix, we explain in detail the process of linearizing the master equation (3), which we reproduce here for convenience,

$$\frac{d\hat{\rho}}{dt} = \left[\frac{\hat{H}_{\text{OM}}}{i\hbar},\hat{\rho}\right] + \gamma\mathcal{D}_{b_1}[\hat{\rho}] + \Gamma\mathcal{D}_a[\hat{\rho}], \qquad \text{(B1)}$$

with

$$\frac{\hat{H}_{\text{OM}}}{\hbar} = \nu\hat{a}^\dagger\hat{a} + [\Delta_1 - g_0\hat{x}]\hat{b}_1^\dagger\hat{b}_1 - (\mathcal{E}^*\hat{b}_1 + \mathcal{E}\hat{b}_1^\dagger), \qquad \text{(B2a)}$$

$$\mathcal{D}_J[\hat{\rho}] = 2\hat{J}\hat{\rho}\hat{J}^\dagger - \hat{J}^\dagger\hat{J}\hat{\rho} - \hat{\rho}\hat{J}^\dagger\hat{J}. \qquad \text{(B2b)}$$

1. The classical limit

Linearization consists in considering small quantum fluctuations around the classical state of the system. Hence, we first consider here the classical limit, which in this case is obtained by assuming that the state is a product of coherent states for both modes: $|\alpha\rangle\otimes|\beta\rangle$, where $\hat{a}|\alpha\rangle = \alpha|\alpha\rangle$ and $\hat{b}_1|\beta\rangle = \beta|\beta\rangle$. The master equation can then be turned into an evolution equation for the coherent amplitudes $\alpha(t)$ and $\beta(t)$. Let us find such equation.

In order to do this, it is convenient to first note that the evolution equation of the expectation value of any operator $\hat{A}$ can be written as

$$\begin{aligned}
\frac{d\langle\hat{A}\rangle}{dt} &= \text{tr}\left\{\hat{A}\frac{d\hat{\rho}}{dt}\right\} \\
&= \frac{1}{i\hbar}\langle[\hat{A},\hat{H}_{\text{OM}}]\rangle + \gamma\langle[\hat{b}_1^\dagger,\hat{A}]\hat{b}_1 + \hat{b}_1^\dagger[\hat{A},\hat{b}_1]\rangle \\
&\quad + \Gamma\langle[\hat{a}^\dagger,\hat{A}]\hat{a} + \hat{a}^\dagger[\hat{A},\hat{a}]\rangle. \qquad \text{(B3)}
\end{aligned}$$

Applying this expression to the operators $\hat{a}$ and $\hat{b}_1$, and using the fact that coherent states are their eigenstates, we easily find the evolution equations,

$$\dot{\alpha} = -(\Gamma + i\nu)\alpha + ig_0|\beta|^2, \qquad \text{(B4a)}$$

$$\dot{\beta} = -[\gamma + i\Delta_1 - ig_0(\alpha+\alpha^*)]\beta + i\mathcal{E}. \qquad \text{(B4b)}$$

These evolution equations possess stationary states ($\dot{\alpha} = 0 = \dot{\beta}$) defined by

$$\bar{\alpha} = g_0|\bar{\beta}|^2/(\nu - i\Gamma) \approx g_0|\bar{\beta}|^2/\nu, \qquad \text{(B5a)}$$

$$\bar{\beta} = \mathcal{E}/[\Delta_1 - g_0(\bar{\alpha}+\bar{\alpha}^*) - i\gamma] \approx \mathcal{E}/\nu, \qquad \text{(B5b)}$$

where in the last step we have made use of the regime $\Delta_1 = \nu \gg \max\{g_0|\bar{\beta}|,\gamma,\Gamma\}$ that we showed in the main text to be required for an appropriate beam-splitter operation. This solution must be stable against perturbations in order for linearization to work. Writing $\alpha(t) = \bar{\alpha} + \delta\alpha(t)$ and $\beta(t) = \bar{\beta} + \delta\beta(t)$ in (B4), and keeping terms to first order in the fluctuations, we get

$$\begin{aligned}
\frac{d}{dt}\begin{pmatrix}\delta\alpha\\ \delta\alpha^*\\ \delta\beta\\ \delta\beta^*\end{pmatrix} &= \begin{pmatrix}-\Gamma-i\nu & 0 & ig_0\bar{\beta}^* & ig_0\bar{\beta}\\ 0 & -\Gamma+i\nu & -ig_0\bar{\beta}^* & -ig_0\bar{\beta}\\ ig_0\bar{\beta} & ig_0\bar{\beta} & -\gamma-i\Delta_1+2ig_0\text{Re}\{\bar{\alpha}\} & 0\\ -ig_0\bar{\beta}^* & -ig_0\bar{\beta}^* & 0 & -\gamma+i\Delta_1-2ig_0\text{Re}\{\bar{\alpha}\}\end{pmatrix}\begin{pmatrix}\delta\alpha\\ \delta\alpha^*\\ \delta\beta\\ \delta\beta^*\end{pmatrix} \\
&\approx \underbrace{\begin{pmatrix}-\Gamma-i\nu & 0 & ig_0\bar{\beta}^* & ig_0\bar{\beta}\\ 0 & -\Gamma+i\nu & -ig_0\bar{\beta}^* & -ig_0\bar{\beta}\\ ig_0\bar{\beta} & ig_0\bar{\beta} & -\gamma-i\nu & 0\\ -ig_0\bar{\beta}^* & -ig_0\bar{\beta}^* & 0 & -\gamma+i\nu\end{pmatrix}}_{\mathcal{M}}\begin{pmatrix}\delta\alpha\\ \delta\alpha^*\\ \delta\beta\\ \delta\beta^*\end{pmatrix}, \qquad \text{(B6)}
\end{aligned}$$

where in the last step we have made use of the regime $\Delta_1 = \nu \gg g_0|\bar{\beta}|$ and (B5). The solution will be stable whenever the fluctuations decay towards zero, which in turn happens only if the eigenvalues of $\mathcal{M}$, known as the linear stability matrix, have all negative real part. This is clearly the case for $g_0 = 0$. On the other hand, the terms proportional to $g_0|\bar{\beta}| \ll \nu$ are just a small perturbation which is readily shown to not be able to make the system unstable. Hence, in conclusion, under our operating conditions, it is ensured that the stationary solution (B5) is stable.

2. Linearization of quantum fluctuations

In order to introduce the linearized approximation for quantum fluctuations, we move to a picture displaced to the classical steady state presented above. Defining the displacement $\hat{D}(\bar{\alpha}, \bar{\beta}) = \exp(\bar{\alpha}\hat{a} + \bar{\beta}\hat{b}_1 - \text{H.c.})$ which transforms the bosonic operators as $\hat{D}^\dagger \hat{a} \hat{D} = \hat{a} + \bar{\alpha}$ and $\hat{D}^\dagger \hat{b}_1 \hat{D} = \hat{b}_1 + \bar{\beta}$, the transformed state $\tilde{\rho} = \hat{D}^\dagger \hat{\rho} \hat{D}$ is easily shown to evolve according to the master equation

$$\frac{d\tilde{\rho}}{dt} = \left[\frac{\tilde{H}}{i\hbar}, \tilde{\rho}\right] + \gamma \mathcal{D}_{b_1}[\tilde{\rho}] + \Gamma \mathcal{D}_a[\tilde{\rho}], \tag{B7}$$

with

$$\frac{\tilde{H}}{\hbar} = \nu \hat{a}^\dagger \hat{a} + \tilde{\Delta}_1 \hat{b}_1^\dagger \hat{b}_1 - g_0 \hat{x}(\bar{\beta}\hat{b}_1^\dagger + \bar{\beta}^* \hat{b}_1 + \hat{b}_1^\dagger \hat{b}_1), \tag{B8}$$

with $\tilde{\Delta}_1 = \Delta_1 - g_0(\bar{\alpha} + \bar{\alpha}^*)$. In this picture, the optomechanical interaction has a different form. It contains the bilinear term $g_0\hat{x}(\bar{\beta}\hat{b}_1^\dagger + \bar{\beta}^*\hat{b}_1)$ that we introduced in the text, in addition to the original term $g_0\hat{x}\hat{b}_1^\dagger\hat{b}_1$. It is clear that the latter will be negligible whenever $|\bar{\beta}|^2 \gg \langle \hat{b}_1^\dagger \hat{b}_1 \rangle$. But there is one more way in which it can become negligible: since $\hat{x}$ oscillates at frequency ν, the rotating-wave approximation will suppress it whenever $\nu \gg g_0 \langle \hat{b}_1^\dagger \hat{b}_1 \rangle^{1/2}$. Under any of these conditions, the Hamiltonian can then be approximated by only its bilinear term, as we provided in (5) in the main text. Moreover, working in the regime $\Delta_1 = \nu \gg \max\{g_0|\bar{\beta}|, \gamma, \Gamma\}$ (required for a proper beam-splitter operation) allowed us to made the approximation $\tilde{\Delta}_1 \approx \Delta_1$ in the main text.

APPENDIX C: EFFECT OF PARAMETER FLUCTUATIONS

Here we explain in detail how we have analyzed the effect of parameter fluctuations in our protocol. Note that in order to simplify the expressions and derivations, here we use different conventions as compared to the main text. In particular, we use a different sign convention for the beam-splitter operation, and we start from a state with N photons instead of N phonons. Of course, none of these choices affects the final conclusion.

The basic idea is that instead of considering ideal operations, we consider a beam splitter $\hat{B}_\lambda = \exp[\lambda(\hat{a}\hat{b}_1^\dagger - \hat{a}^\dagger \hat{b}_1)]$ and a controlled-θ $\hat{C}_\theta = \exp(i\theta \hat{b}_2^\dagger \hat{b}_2 \hat{a}^\dagger \hat{a})$ with fluctuating parameters $\lambda = \pi/4 + \delta\lambda$ and $\theta = \pi + \delta\theta$, where both fluctuations $\delta\lambda$ and $\delta\theta$ are taken as Gaussian stochastic processes. Denoting either of them by δz (hence, $z = \lambda, \theta$), we then have

$$\overline{\delta z^n} = \begin{cases} 0 & \text{for } n \in \text{odd} \\ (n-1)!!\, V_z^{n/2} & \text{for } n \in \text{even}, \end{cases} \tag{C1}$$

where V_z is the variance (square of the standard deviation) of the fluctuations, and in the following we denote stochastic averages by an overbar.

As a proof of principle, we then evaluate the (stochastically averaged) fidelity between the ideal and fluctuating states. In order to simplify the calculation, we will consider the states right after the controlled-θ operation instead of at the very end of the protocol. In any case, this will give us a fair idea of the sensitivity of the protocol to parameter fluctuations. Consider then the state at this stage of the protocol, which can be written as

$$\begin{aligned} |\Phi_{\lambda,\theta}\rangle &= \frac{1}{\sqrt{2}} \hat{C}_\theta \hat{B}_\lambda |N\rangle_1 |0\rangle_a (|0\rangle_2 + |1\rangle_2) \\ &= \frac{1}{\sqrt{2}} (|\psi_\lambda\rangle_{1a}|0\rangle_2 + \hat{P}_\theta |\psi_\lambda\rangle_{1a}|1\rangle_2), \end{aligned} \tag{C2}$$

where $\hat{P}_\theta = e^{i\theta \hat{a}^\dagger \hat{a}}$ and

$$\begin{aligned} |\psi_\lambda\rangle_{1a} &= \hat{B}_\lambda |N\rangle_1 |0\rangle_a \\ &= \sum_{k=0}^{N} \sqrt{\binom{N}{k}} \sin^k \lambda \cos^{N-k} \lambda |N-k\rangle_1 |k\rangle_a. \end{aligned} \tag{C3}$$

The overlap between this state and the ideal one $|\Phi_{\pi/4,\pi}\rangle$ is then given by

$$\langle \Phi_{\pi/4,\pi} | \Phi_{\lambda,\theta} \rangle = \tfrac{1}{2}(\langle \psi_{\pi/4} | \psi_\lambda \rangle_{1a} + \langle \psi_{\pi/4} | \hat{P}_{\delta\theta} | \psi_\lambda \rangle_{1a}), \tag{C4}$$

where we have used $\hat{P}_\pi^\dagger \hat{P}_\theta = \hat{P}_{\delta\theta}$. Using (C3), these two terms are easily rewritten as

$$\langle \psi_{\pi/4} | \psi_\lambda \rangle_{1a} = \sum_{k=0}^{N} \frac{1}{\sqrt{2^N}} \binom{N}{k} \sin^k \lambda \cos^{N-k} \lambda, \tag{C5a}$$

$$\langle \psi_{\pi/4} | \hat{P}_{\delta\theta} | \psi_\lambda \rangle_{1a} = \sum_{k=0}^{N} \frac{1}{\sqrt{2^N}} \binom{N}{k} e^{ik\delta\theta} \sin^k \lambda \cos^{N-k} \lambda, \tag{C5b}$$

so that

$$\langle \Phi_{\pi/4,\pi} | \Phi_{\lambda,\theta} \rangle = \sum_{k=0}^{N} \frac{1 + e^{ik\delta\theta}}{2\sqrt{2^N}} \binom{N}{k} \sin^k \lambda \cos^{N-k} \lambda. \tag{C6}$$

On the other hand, the average fidelity can be evaluated as

$$\mathcal{F} = \overline{|\langle \Phi_{\pi/4,\pi} | \Phi_{\lambda,\theta} \rangle|}, \tag{C7}$$

that is, the average of the absolute value of the overlap. Let us then now perform the required stochastic averages. First, let us note that

$$\begin{aligned} \overline{\sin^n \lambda \cos^m \lambda} = \frac{1}{2^{n+m} i^n} \sum_{l=0}^{n} \sum_{l'=0}^{m} (-1)^l \binom{n}{l} \binom{m}{l'} \\ \times e^{i\pi(n+m-2l-2l')/4} e^{-(n+m-2l-2l')^2 V_\lambda/2}, \end{aligned} \tag{C8}$$

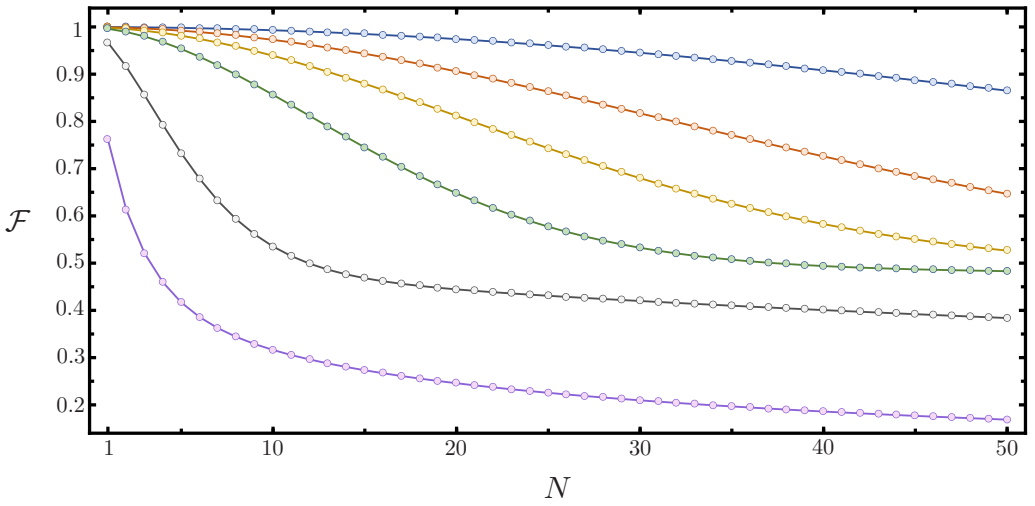

FIG. 3. Fidelity of the state generated by our protocol as a function of the NOON size N, and for different values of the standard deviation of the beam splitter and controlled-π parameters: 1% (blue), 2% (orange), 3% (yellow), 5% (green), 15% (gray), and 50% (purple), from top to bottom.

which are expressions that we prove at the end of the section. Hence, we can write

$$\begin{aligned}\overline{\langle\Phi_{\pi/4,\pi}|\Phi_{\lambda,\theta}\rangle} &= \sum_{k=0}^{N}\frac{1}{2\sqrt{2^N}}\binom{N}{k}(1+\overline{e^{ik\delta\theta}})\overline{\sin^k\lambda\cos^{N-k}\lambda}\\ &= \sum_{k=0}^{N}\frac{1}{2\sqrt{2^N}}\binom{N}{k}(1+e^{-k^2V_\theta/2})\frac{1}{2^N i^k}\sum_{l=0}^{k}\sum_{l'=0}^{N-k}(-1)^l\binom{k}{l}\binom{N-k}{l'}e^{i\pi(N-2l-2l')/4}e^{-(N-2l-2l')^2V_\lambda/2}\\ &= \sum_{k=0}^{N}\sum_{l=0}^{k}\sum_{l'=0}^{N-k}\frac{(-1)^l}{2^{1+3N/2}i^k}\binom{N}{k}\binom{k}{l}\binom{N-k}{l'}e^{i\pi(N-2l-2l')/4}(1+e^{-k^2V_\theta/2})e^{-(N-2l-2l')^2V_\lambda/2},\end{aligned}\tag{C9}$$

which is an expression that can be evaluated very efficiently by any computer.

In Fig. 3, we plot the fidelity (C7) as a function of N for different values of the standard deviation of the parameters. As mentioned in the main text, for 1% standard deviation, the fidelity stays above 90% for values as large as $N = 40$. Note that the standard deviation is the square root of the variance and, hence, M% means $V_\theta = (10^{-2}M\pi)^2$ and $V_\lambda = (10^{-2}M\pi/4)^2$.

Let us now prove expressions (C8). In the case of the first one, we simply expand the exponential in a Taylor series and use (C1), leading to

$$\begin{aligned}\overline{e^{inz}} &= \sum_{k=0}^{\infty}\frac{1}{k!}(in)^k\overline{z^k} = \sum_{l=0}^{\infty}\frac{(2l-1)!!}{(2l)!}(in)^{2l}V_z^l\\ &= \sum_{l=0}^{\infty}\frac{1}{2^l l!}(-n^2)^l V_z^l = e^{-n^2V_z/2}.\end{aligned}\tag{C10}$$

As for the second expression, it is also easy to prove by writing the trigonometric functions in terms of complex exponentials and using the previous expression:

$$\begin{aligned}\overline{\sin^n\lambda\cos^m\lambda} &= \frac{1}{2^{n+m}i^n}\overline{(e^{i\lambda}-e^{-i\lambda})^n(e^{i\lambda}+e^{-i\lambda})^m}\\ &= \frac{1}{2^{n+m}i^n}\sum_{l=0}^{n}\sum_{l'=0}^{m}(-1)^l\binom{n}{l}\binom{m}{l'}\overline{e^{i(n+m-2l-2l')\lambda}}\\ &= \frac{1}{2^{n+m}i^n}\sum_{l=0}^{n}\sum_{l'=0}^{m}(-1)^l\binom{n}{l}\binom{m}{l'}\\ &\quad\times e^{i\pi(n+m-2l-2l')/4}e^{-(n+m-2l-2l')^2V_\lambda/2}.\end{aligned}\tag{C11}$$

[1] C. Gross and I. Bloch, Science **357**, 995 (2017).
[2] I. Bloch, J. Dalibard, and S. Nascimbene, Nat. Phys. **8**, 267 (2012).
[3] I. Bloch, J. Dalibard, and W. Zwerger, Rev. Mod. Phys. **80**, 885 (2008).
[4] A. Keesling, A. Omran, H. Levine, H. Bernien, H. Pichler, S. Choi, R. Samajdar, S. Schwartz, P. Silvi, S. Sachdev, P. Zoller,

M. Endres, M. Greiner, V. Vuletić, and M. D. Lukin, Nature (London) **568**, 207 (2019).
[5] H. Bernien, S. Schwartz, A. Keesling, H. Levine, A. Omran, H. Pichler, S. Choi, A. S. Zibrov, M. Endres, M. Greiner, V. Vuletić, and M. D. Lukin, Nature (London) **551**, 579 (2017).
[6] M. Endres, H. Bernien, A. Keesling, H. Levine, E. R. Anschuetz, A. Krajenbrink, C. Senko, V. Vuletic, M. Greiner, and M. D. Lukin, Science **354**, 1024 (2016).
[7] V. Lienhard, S. de Léséleuc, D. Barredo, T. Lahaye, A. Browaeys, M. Schuler, L.-P. Henry, and A. M. Läuchli, Phys. Rev. X **8**, 021070 (2018).
[8] T. L. Nguyen, J. M. Raimond, C. Sayrin, R. Cortiñas, T. Cantat-Moltrecht, F. Assemat, I. Dotsenko, S. Gleyzes, S. Haroche, G. Roux, T. Jolicoeur, and M. Brune, Phys. Rev. X **8**, 011032 (2018).
[9] N. Mohseni, M. Fani, J. P. Dowling, and S. Saeidian, Phys. Rev. A **96**, 013859 (2017).
[10] M. Saffman, J. Phys. B: At., Mol. Opt. Phys. **49**, 202001 (2016).
[11] A. Negretti, P. Treutlein, and T. Calarco, Quantum Inf. Proc. **10**, 721 (2011).
[12] P. S. Jessen, R. Stock *et al.*, Quantum Inf. Proc. **3**, 91 (2004).
[13] L. Pezzè, A. Smerzi, M. K. Oberthaler, R. Schmied, and P. Treutlein, Rev. Mod. Phys. **90**, 035005 (2018).
[14] S. Bize, C. R. Phys. **20**, 153 (2019).
[15] G. E. Marti, R. B. Hutson, A. Goban, S. L. Campbell, N. Poli, and J. Ye, Phys. Rev. Lett. **120**, 103201 (2018).
[16] A. Mann, Proc. Natl. Acad. Sci. USA **115**, 7449 (2018).
[17] J. P. Dowling, Contemp. Phys. **49**, 125 (2008).
[18] V. Paulisch, M. Perarnau-Llobet, A. González-Tudela, and J. I. Cirac, Phys. Rev. A **99**, 043807 (2019).
[19] A. Omran, H. Levine, A. Keesling, G. Semeghini, T. T. Wang, S. Ebadi, H. Bernien, A. S. Zibrov, H. Pichler, S. Choi, J. Cui, M. Rossignolo, P. Rembold, S. Montangero, T. Calarco, M. Endres, M. Greiner, V. Vuletić, and M. D. Lukin, Science **365**, 570 (2019).
[20] T. Monz, P. Schindler, J. T. Barreiro, M. Chwalla, D. Nigg, W. A. Coish, M. Harlander, W. Hänsel, M. Hennrich, and R. Blatt, Phys. Rev. Lett. **106**, 130506 (2011).
[21] X.-L. Wang, L.-K. Chen, W. Li, H.-L. Huang, C. Liu, C. Chen, Y.-H. Luo, Z.-E. Su, D. Wu, Z.-D. Li, H. Lu, Y. Hu, X. Jiang, C.-Z. Peng, L. Li, N.-L. Liu, Y.-A. Chen, C.-Y. Lu, and J.-W. Pan, Phys. Rev. Lett. **117**, 210502 (2016).
[22] I. Afek, O. Ambar, and Y. Silberberg, Science **328**, 879 (2010).
[23] J. Zhang, M. Um, D. Lv, J.-N. Zhang, L.-M. Duan, and K. Kim, Phys. Rev. Lett. **121**, 160502 (2018).
[24] J. M. Raimond, M. Brune, and S. Haroche, Rev. Mod. Phys. **73**, 565 (2001).
[25] S. Haroche, Nobel Lecture (2012), www.nobelprize.org.
[26] A. Cooper, J. P. Covey, I. S. Madjarov, S. G. Porsev, M. S. Safronova, and M. Endres, Phys. Rev. X **8**, 041055 (2018).
[27] H. Levine, A. Keesling, A. Omran, H. Bernien, S. Schwartz, A. S. Zibrov, M. Endres, M. Greiner, V. Vuletić, and M. D. Lukin, Phys. Rev. Lett. **121**, 123603 (2018).
[28] J. D. Thompson, T. G. Tiecke, A. S. Zibrov, V. Vuletić, and M. D. Lukin, Phys. Rev. Lett. **110**, 133001 (2013).
[29] M. A. Norcia, A. W. Young, and A. M. Kaufman, Phys. Rev. X **8**, 041054 (2018).
[30] A. M. Kaufman, B. J. Lester, C. M. Reynolds, M. L. Wall, M. Foss-Feig, K. R. A. Hazzard, A. M. Rey, and C. A. Regal, Science **345**, 306 (2014).
[31] A. M. Kaufman, B. J. Lester, and C. A. Regal, Phys. Rev. X **2**, 041014 (2012).
[32] D. Barredo, S. de Léséleuc, V. Lienhard, T. Lahaye, and A. Browaeys, Science **354**, 1021 (2016).
[33] A. Browaeys, D. Barredo, and T. Lahaye, J. Phys. B: At., Mol. Opt. Phys. **49**, 152001 (2016).
[34] H. Labuhn, D. Barredo, S. Ravets, S. de Léséleuc, T. Macrì, T. Lahaye, and A. Browaeys, Nature (London) **534**, 667 (2016).
[35] S. K. Dutta, J. R. Guest, D. Feldbaum, A. Walz-Flannigan, and G. Raithel, Phys. Rev. Lett. **85**, 5551 (2000).
[36] K. C. Younge, B. Knuffman, S. E. Anderson, and G. Raithel, Phys. Rev. Lett. **104**, 173001 (2010).
[37] S. E. Anderson, K. C. Younge, and G. Raithel, Phys. Rev. Lett. **107**, 263001 (2011).
[38] K. C. Younge, S. E. Anderson, and G. Raithel, New J. Phys. **12**, 023031 (2010).
[39] S. Zhang, F. Robicheaux, and M. Saffman, Phys. Rev. A **84**, 043408 (2011).
[40] L. Li, Y. O. Dudin, and A. Kuzmich, Nature (London) **498**, 466 (2013).
[41] D. Barredo, V. Lienhard, P. Scholl, S. de Léséleuc, T. Boulier, A. Browaeys, and T. Lahaye, arXiv:1908.00853.
[42] D. Leibfried, R. Blatt, C. Monroe, and D. Wineland, Rev. Mod. Phys. **75**, 281 (2003).
[43] D. J. Wineland, Nobel Lecture (2012), www.nobelprize.org.
[44] C. C. Gerry and R. A. Campos, Phys. Rev. A **64**, 063814 (2001).
[45] D. M. Meekhof, C. Monroe, B. E. King, W. M. Itano, and D. J. Wineland, Phys. Rev. Lett. **76**, 1796 (1996).
[46] D. Kienzler, H.-Y. Lo, V. Negnevitsky, C. Flühmann, M. Marinelli, and J. P. Home, Phys. Rev. Lett. **119**, 033602 (2017).
[47] M. Um, J. Zhang, D. Lv, Y. Lu, S. An, J.-N. Zhang, H. Nha, M. S. Kim, and K. Kim, Nat. Commun. **7**, 11410 (2016).
[48] A. Ben-Kish, B. DeMarco, V. Meyer, M. Rowe, J. Britton, W. M. Itano, B. M. Jelenković, C. Langer, D. Leibfried, T. Rosenband, and D. J. Wineland, Phys. Rev. Lett. **90**, 037902 (2003).
[49] B. Peaudecerf, C. Sayrin, X. Zhou, T. Rybarczyk, S. Gleyzes, I. Dotsenko, J. M. Raimond, M. Brune, and S. Haroche, Phys. Rev. A **87**, 042320 (2013).
[50] X. Zhou, I. Dotsenko, B. Peaudecerf, T. Rybarczyk, C. Sayrin, S. Gleyzes, J. M. Raimond, M. Brune, and S. Haroche, Phys. Rev. Lett. **108**, 243602 (2012).
[51] C. Sayrin, I. Dotsenko, B. Peaudecerf, T. Rybarczyk, S. Gleyzes, P. Rouchon, M. Mirrahimi, H. Amini, M. Brune, J.-M. Raimond, and S. Haroche, Nature (London) **477**, 73 (2011).
[52] B. T. Varcoe, S. Brattke, M. Weidinger, and H. Walther, Nature (London) **403**, 743 (2000).
[53] X. Luo, X. Zhu, Y. Wu, M. Feng, and K. Gao, Phys. Lett. A **237**, 354 (1998).
[54] F. Mintert and C. Wunderlich, Phys. Rev. Lett. **87**, 257904 (2001).
[55] M. Johanning, A. Braun, N. Timoney, V. Elman, W. Neuhauser, and C. Wunderlich, Phys. Rev. Lett. **102**, 073004 (2009).
[56] A. Khromova, C. Piltz, B. Scharfenberger, T. F. Gloger, M. Johanning, A. F. Varón, and C. Wunderlich, Phys. Rev. Lett. **108**, 220502 (2012).
[57] C. Piltz, T. Sriarunothai, A. F. Varón, and C. Wunderlich, Nat. Commun. **5**, 4679 (2014).
[58] C. Piltz, T. Sriarunothai, S. S. Ivanov, S. Wölk, and C. Wunderlich, Sci. Adv. **2**, e1600093 (2016).

[59] S. Wölk and C. Wunderlich, New J. Phys. **19**, 083021 (2017).
[60] T. Sriarunothai, G. S. Giri, S. Wölk, and C. Wunderlich, J. Mod. Opt. **65**, 560 (2018).
[61] K. Lake, S. Weidt, J. Randall, E. D. Standing, S. C. Webster, and W. K. Hensinger, Phys. Rev. A **91**, 012319 (2015).
[62] S. Weidt, J. Randall, S. C. Webster, K. Lake, A. E. Webb, I. Cohen, T. Navickas, B. Lekitsch, A. Retzker, and W. K. Hensinger, Phys. Rev. Lett. **117**, 220501 (2016).
[63] C. Ospelkaus, C. E. Langer, J. M. Amini, K. R. Brown, D. Leibfried, and D. J. Wineland, Phys. Rev. Lett. **101**, 090502 (2008).
[64] C. Ospelkaus, U. Warring, Y. Colombe, K. R. Brown, J. M. Amini, D. Leibfried, and D. J. Wineland, Nature (London) **476**, 181 (2011).
[65] L. Förster, M. Karski, J.-M. Choi, A. Steffen, W. Alt, D. Meschede, A. Widera, E. Montano, J. H. Lee, W. Rakreungdet, and P. S. Jessen, Phys. Rev. Lett. **103**, 233001 (2009).
[66] X. Li, T. A. Corcovilos, Y. Wang, and D. S. Weiss, Phys. Rev. Lett. **108**, 103001 (2012).
[67] N. Belmechri, L. Förster, W. Alt, A. Widera, D. Meschede, and A. Alberti, J. Phys. B: At., Mol. Opt. Phys. **46**, 104006 (2013).
[68] B. Albrecht, Y. Meng, C. Clausen, A. Dareau, P. Schneeweiss, and A. Rauschenbeutel, Phys. Rev. A **94**, 061401(R) (2016).
[69] A. B. Bhattacherjee, Int. J. Theor. Phys. **55**, 1944 (2016).
[70] M. Aspelmeyer, T. J. Kippenberg, and F. Marquardt, Rev. Mod. Phys. **86**, 1391 (2014).
[71] F. L. Semiao and A. Vidiella-Barranco, Phys. Rev. A **72**, 064305 (2005).
[72] F. Assemat, D. Grosso, A. Signoles, A. Facon, I. Dotsenko, S. Haroche, J. M. Raimond, M. Brune, and S. Gleyzes, Phys. Rev. Lett. **123**, 143605 (2019).
[73] C. Maurer, C. Becher, C. Russo, J. Eschner, and R. Blatt, New J. Phys. **6**, 94 (2004).